Open conformation of human DOPA decarboxylase reveals the mechanism of PLP addition to Group II decarboxylases

Giorgio Giardina[a], Riccardo Montioli[b], Stefano Gianni[c], Barbara Cellini[b], Alessandro Paiardini[a], Carla Borri Voltattorni[b,1], and Francesca Cutruzzolà[a,d,1]

[a]Dipartimento di Scienze Biochimiche 'A. Rossi Fanelli', Sapienza Università di Roma, Piazzale Aldo Moro 5, 00185 Rome, Italy; [b]Dipartimento di Scienze della Vita e della Riproduzione, Sezione di Chimica Biologica, Facoltà di Medicina e Chirurgia, Università degli Studi di Verona, Strada Le Grazie, 8, 37134 Verona, Italy; [c]Istituto di Biologia e Patologia Molecolari del Consiglio Nazionale delle Ricerche, Dipartimento di Scienze Biochimiche 'A. Rossi Fanelli', Sapienza Università di Rome, Piazzale Aldo Moro 5, 00185 Rome, Italy; and [d]Istituto Pasteur Fondazione Cenci Bolognetti, Dipartimento di Scienze Biochimiche 'A. Rossi Fanelli', Sapienza Università di Roma, Piazzale Aldo Moro 5, 00185 Rome, Italy

Edited by Harry B. Gray, California Institute of Technology, Pasadena, CA, and approved October 3, 2011 (received for review July 14, 2011)

DOPA decarboxylase, the dimeric enzyme responsible for the synthesis of neurotransmitters dopamine and serotonin, is involved in severe neurological diseases such as Parkinson disease, schizophrenia, and depression. Binding of the pyridoxal-5′-phosphate (PLP) cofactor to the apoenzyme is thought to represent a central mechanism for the regulation of its activity. We solved the structure of the human apoenzyme and found it exists in an unexpected open conformation: compared to the pig kidney holoenzyme, the dimer subunits move 20 Å apart and the two active sites become solvent exposed. Moreover, by tuning the PLP concentration in the crystals, we obtained two more structures with different conformations of the active site. Analysis of three-dimensional data coupled to a kinetic study allows to identify the structural determinants of the open/close conformational change occurring upon PLP binding and thereby propose a model for the preferential degradation of the apoenzymes of Group II decarboxylases.

apoprotein | Shiff base | stability | kinetics | FRET

Dopamine, serotonin, GABA, and histamine are synthesized by three structurally related pyridoxal-5′-phosphate (PLP) dependent enzymes: 3,4-dihydroxy-L-phenylalanin (L-DOPA) decarboxylase (DDC), the glutamic acid decarboxylase (GAD), and the histidine decarboxylase (HDC). These enzymes belong to the Group II of Fold Type I aspartate aminotransferase family. Surprisingly, despite these three decarboxylases are involved in severe diseases [e.g., Parkinson's disease, Tourette's syndrome, schizophrenia, depression and cancer (1–5)], the regulation of their activity is still shrouded in mystery.

In the brain, where the three enzymes are highly expressed (6, 7), the equilibrium between apo- and holoenzymes is dependent on PLP availability (8–10). Binding of PLP to the apoenzymes is thought to represent an essential mechanism of their regulation (11) and altered ratio of holo- vs. apoenzymes, as well as preferential degradation of the latter, have been implied in a number of diseases and disorders such as DDC deficiency (12–14). PLP crosses the blood brain barrier as its vitamin B_6 precursors, Pyridoxal (PL), Pyridoxine (PN), or Pyridoxamine (PM) and then is phosphorylated again by the pyridoxal kinase (PLK) (15, 16). Therefore vitamin B_6 deficiency in the central nervous system (CNS) or inherited defects in the gene encoding PLK, are also responsible for the alteration in the equilibrium between apo- and holo-decarboxylases, and represent the cause of several neurological pathologies [e.g., epilepsy, EEG abnormalities, psychiatric disorders (13, 17)]. However, there is still little understanding of the mechanism of PLP binding to the apoenzymes. It has been suggested that, upon PLP binding, the three decarboxylases undergo a large conformational change, which leads to a more compact and less solvent accessible conformation (18–21). Nevertheless there are still many obscure points: (*i*) What is the exact mechanism of PLP binding to Group II apo- decarboxylases? (*ii*) How large is the conformational difference between the holo- and apo-forms? (*iii*) What is the reason behind the preferential degradation of the latter? (*iv*) Does the apoenzyme bind to free PLP in vivo or does this happen through a protein-protein interaction with PLK? To date, no clues to address these puzzling issues have come from structural biology, because no experimentally determined apo-structure of the Group II enzymes had been obtained so far.

Here we present the crystal structure of an apoenzyme of Group II decarboxylases; the human apoDDC. Based on structural and kinetic data, we could identify the structural determinants of the conformational change occurring upon PLP binding and propose a model for the preferential degradation of the apoenzyme. Our results force to reconsider the mechanism of PLP addition to the apoenzymes of Group II decarboxylases in a ~~unique~~ perspective. Insights coming from this structural work may thus prove fundamental in understanding the regulation of the homeostasis of this key class of enzymes in the CNS and in the peripheral tissues, and will hopefully help to develop new therapeutical approaches.

Results

Group II decarboxylases are homodimers with each monomer composed of three domains (22). The first two, a large domain (L-domain) formed by a central seven-stranded β-sheet surrounded by α-helices and the C-terminal domain (small domain or C-domain), are typical of the aspartate aminotransferase family (Fold Type I). The third N-terminal domain (N-domain) is formed by three α-helices that fold upon dimerization and is characteristic of Group II decarboxylases (22, 23). In the holo structures the active site is buried in the central part of the dimer and accessible only through a tight gorge (18, 24, 25).

In an attempt to investigate, by X-ray crystallography, the structural basis of PLP binding to human apoDDC, we setup a number of crystallization trials using both the apoenzyme and the holoenzyme, the latter in the presence of primary amines. We obtained crystals by mixing the holoDDC with Jeffamine®

Author contributions: G.G., C.B.V., and F.C. designed research; G.G., R.M., S.G., B.C., and F.C.Q:1 performed research; R.M., B.C., and C.B.V. contributed new reagents/analytic tools; G.G., S.G., A.P., C.B.V., and F.C. analyzed data; and G.G., S.G., A.P., C.B.V., and F.C. wrote the paper.

The authors declare no conflict of interest.

This article is a PNAS Direct Submission.

Data deposition: The atomic coordinates have been deposited in the Protein Data Bank, www.pdb.org (PDB ID codes 3RBF; 3RCH; and 3RBL).

[1]To whom correspondence may be addressed. E-mail: francesca.cutruzzola@uniroma1.it or carla.borrivoltattorni@univr.it.

This article contains supporting information online at www.pnas.org/lookup/suppl/doi:10.1073/pnas.1111456108/-/DCSupplemental.

ED-2001 [O,O-Bis (2-aminopropyl) polypropylene glycol]. This precipitant contains primary amino groups attached to the terminus of a polyether backbone. The exchange reaction led to the release of the PLP cofactor bound to the holoprotein yielding crystals of the apoenzyme.

Human apoDDC Crystal Structure: an Open Conformation. Comparison of the human apoDDC (apo-hDDC) with that of the close orthologue pig kidney holoDDC [holo-pkDDC—89% sequence identity (25)] reveals the existence of unexpected conformation because the apo-dimer is completely open with the two large domains moving by up to 20 Å with respect to the holo-enzyme as shown in Fig. 1. The open conformation of the enzyme is achieved through a rigid body quaternary rearrangement of the dimer because the fold of each domain is essentially unchanged in the apo-hDDC. Accordingly, the comparison of near-UV CD spectra as well as of intrinsic and 1-anilinonaphtalene-sulfonic acid (ANS) fluorescence spectra of holo and apo-hDDC provide evidence for different conformations of the two forms (Fig. S1). Such an open form of the apoenzyme could hardly be predicted, because this dramatic conformational rearrangement results in a complete exposure of the active site and hydrophobic regions of the apoDDC. Surprisingly, the dimer interface of the open conformation comprises only the helices of the N-domain (blue in Fig. 1). These helices form an extended helix-bundle with the partner subunit (Fig. S2, Movie S1), while the central part of the L-domain (yellow in Fig. 1) is completely exposed to the solvent. Overall, we can compare the apo-hDDC structure to an open bivalve shell, with the interface between the N-domains functioning as the hinge. Given the reduced dimer interface, the open form of the enzyme may well be representative of a system of conformations where the two monomers are substantially mobile in vivo.

An Asymmetric Structure: Trapping Different Conformations of the Active Site. The crystal form of the open hDDC obtained in Jeffamine® proved to be an extremely powerful system to investigate PLP binding, uncoupling local structural changes in the active site from quaternary conformational changes (i.e., open-closed transition). This uncoupling occurs because, within the crystal lattice, the dimer is trapped in the open conformation by intermolecular crystal contacts (Fig. S3*A*). Moreover, the structure of the two subunits is not symmetrical, with chain-A being more closed than chain-B (Fig. S3*B*).

Indeed, in the first structure that we solved (structure 1 in Fig. 2), the PLP present in the crystallization solution (equimolar to the protein) is still able to bind to the active site, and electron density compatible with PLP was observed in one monomer (chain-A) and was included in the final model with occupancy of 0.5 (Fig. 2). Excitingly, the structural asymmetry of the two subunits is also reflected at the level of the active site, with chain-A appearing able to better accommodate the cofactor than chain-B. This initial observation was confirmed by varying the PLP concentration in the crystals of the open DDC, by soaking. We obtained two more structures of the open enzyme with PLP

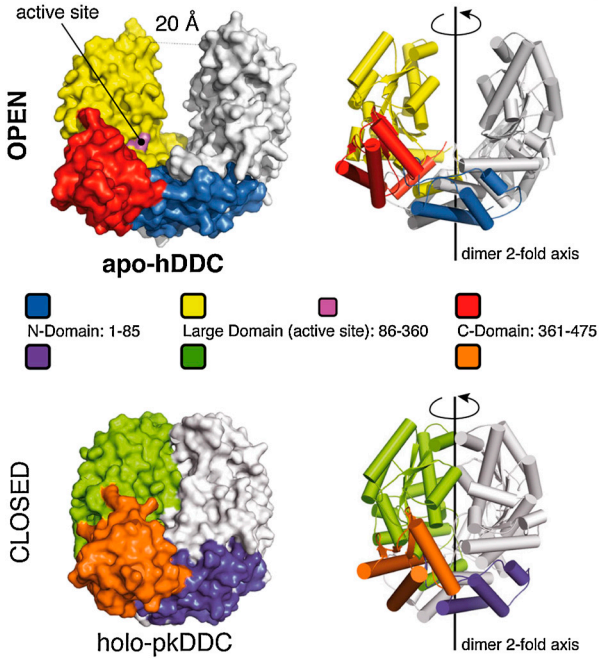

Fig. 1. The apo hDDC open conformation. Surface and cartoon representation of the apo-hDDC structure in the open conformation. The domain organization of one monomer is highlighted using different colors (*Blue*—N-domain; *Yellow*—Large domain; *Red*—C-domain) while the other monomer is shown in *White*. The structure of the holo-pkDDC (pdb id: 1js6) in the closed conformation is shown for comparison in the same orientation; the three domains are colored differently for clarity (*Purple*—N-domain; *Green*—Large domain; *Orange*—C-domain)

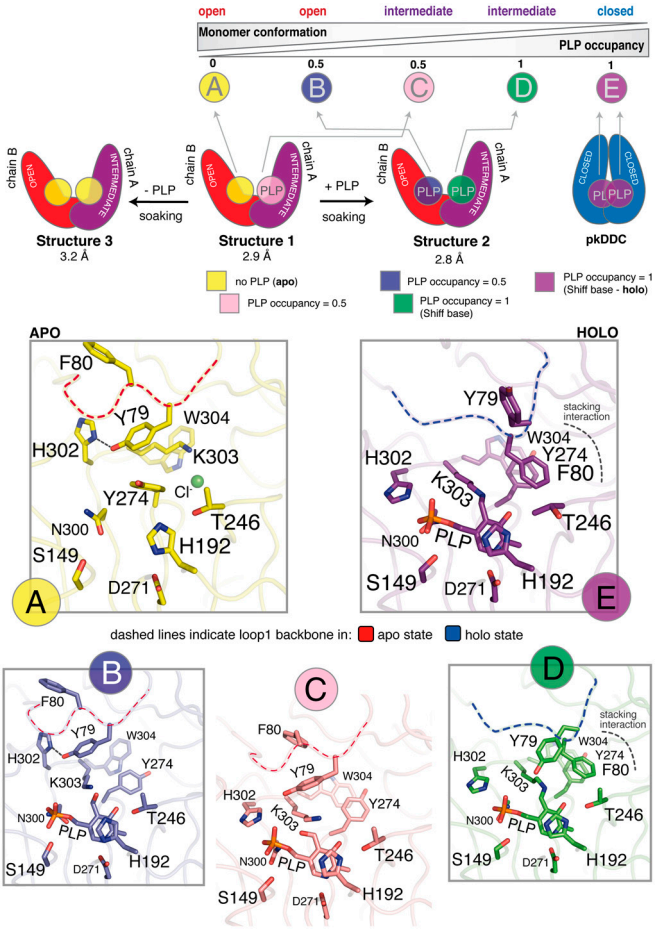

Fig. 2. The asymmetric structure of the open hDDC dimer. The upper part of the figure schematically illustrates the two asymmetric monomers of the open structures of hDDC (*Red*—chain-B, open conformation; *Purple*—chain-A, intermediate conformation; see also Fig. S3) and the PLP occupancy in the four alternative conformations observed for the active site in the three structures of hDDC obtained before (structure 1) and after soaking (structure 2 and 3). Each conformation is shown with different colors and ordered (from *A* to *E*) as illustrated in the scheme, going from the open to the closed monomer (*Blue*—holo-pkDDC, pdb id: 1js6) and from 0 to 1 PLP occupancy. The lower part of the figure shows a stick representation of the side chains of the active site residues in the five alternative conformations, including the closed conformation. The colors used in each box from A to E are the same of the upper scheme. Throughout the boxes a dashed line indicates the position of the backbone residues of loop1: *Red*—apo state; *Blue*—holo state.

bound to both monomers and with no PLP bound respectively (structures 2 and 3 in Fig. 2).

As a consequence of the conformational asymmetry, from the three structures that we solved we identified four alternative conformations of the active site, as illustrated in Fig. 2: (Fig. 2*A*) no PLP (apo); (Fig. 2*B*) 0.5 occupancy of PLP in the open monomer (no internal aldimine formed yet); (Fig. 2*C*) 0.5 occupancy of PLP in the intermediate monomer (no internal aldimine formed yet) and; (Fig. 2*D*) PLP bound with 1.0 occupancy (internal aldimine formed) to the intermediate monomer. These four structures of the active site together with that of the closed-holo-pkDDC, represent a set of five alternative conformations. We have ordered the five structures of the active site according to two parameters: the increase of PLP occupancy and the opening degree of the single monomer (going from Fig. 2 *A* to *E*). These structural snapshots of the active site within the open dimer allowed us to highlight some important structural determinants of the conformational rearrangement upon PLP binding (see Movie S2 online, for a five step morphing from state *A* to *E*, and Fig. S4 for a stereo representation of the electron density of the 4 different conformations).

The starting and the ending point of this set of conformations are the open-apo state (chain-B—structure 1—Fig. 2*A*) and the closed-holo state (Fig. 2*E*—pkDDC structure) respectively. Chain B of structure 1 shows a clear electron density for all the residues in the active site. No density is observed for PLP and thus this subunit may be regarded as a model for the apoprotein open active site. Comparison with the holoprotein (pkDDC) shows that all the major differences are related to the alternative conformation adopted by the last seven residues of loop1 (residues 66–84; connecting the N-domain to the L-domain) and especially by Tyr-79 and Phe-80 in the apo structure. In the apoprotein, Tyr-79 is making a hydrogen bond with His-302 that, as a result, is found in a different conformation than in pkDDC. The side chain of the PLP-binding residue Lys-303 is shifted by 6 Å, swapping its position with that of the rotated side chain of Tyr-274. As a consequence of these changes the favorable aromatic stacking interaction between Trp-304, Tyr-274 and Phe-80, present in the holoenzyme, is disrupted.

Between the open-apo and the closed-holo state, we have trapped three more conformations of the active site (Fig. 2 *B–D*). In the second conformation (Fig. 2*B*—chain-B—structure 2) the steric hindrance of the pyridine ring of PLP, entering in the active site of the open monomer, forces the side chain of Tyr-274 to swap position with Lys-303, which becomes available for aldimine formation.

Moving to the intermediate monomer (Fig. 2*C*—chain-A—structure 1) PLP is bound as in *B* but, as a consequence of the more closed conformation, the catalytic loop (residues 300 to 310) is closer to the PLP molecule. His-302 is back to the position observed in the holo state interacting with the phosphate group, and Tyr-79 is released from the hydrogen bonding interaction. Two out of the three residues involved in the aromatic stacking interaction (Trp-304 and Tyr-274) are positioned as in the holo state of pkDDC, while the third (Phe-80) is in the apo state. Loop1 is still in the apo conformation but is now more mobile as reflected by the increase of the temperature factors and by the reduced occupancy of both Tyr-79 and Phe-80 side chain atoms.

The same monomer after soaking with PLP (Fig. 2*D*—chain-A—structure 2) shows a clear electron density for all PLP atoms and for the double bond of the Shiff base. The structure of the active site is now almost identical to the holo state of pkDDC. Loop1 has completely rearranged to yield the holo state conformation and Phe-80 side chain is now forming the aromatic stacking interaction with Trp-304 and Tyr-274, like in the closed pkDDC structure. The only difference with the closed-holo state is the position of the Tyr-79 side chain, which in the open structures is solvent exposed and thus not well defined.

PLP Binding to the apo-hDDC. Similar to the pig kidney enzyme, human DDC binds PLP with high affinity ($K_D = 43nM$) (26). We followed the kinetics of PLP binding to apo-hDDC by stopped-flow experiments under pseudo-first-order conditions at a constant protein concentration and at different cofactor concentrations (Fig. 3). Because PLP is also a fluorophore, exciting at 280 nm results in a Forster resonance energy transfer (FRET) between the enzyme aromatic residues (donors) and the PLP (acceptor). We followed both the donors and the acceptor fluor-

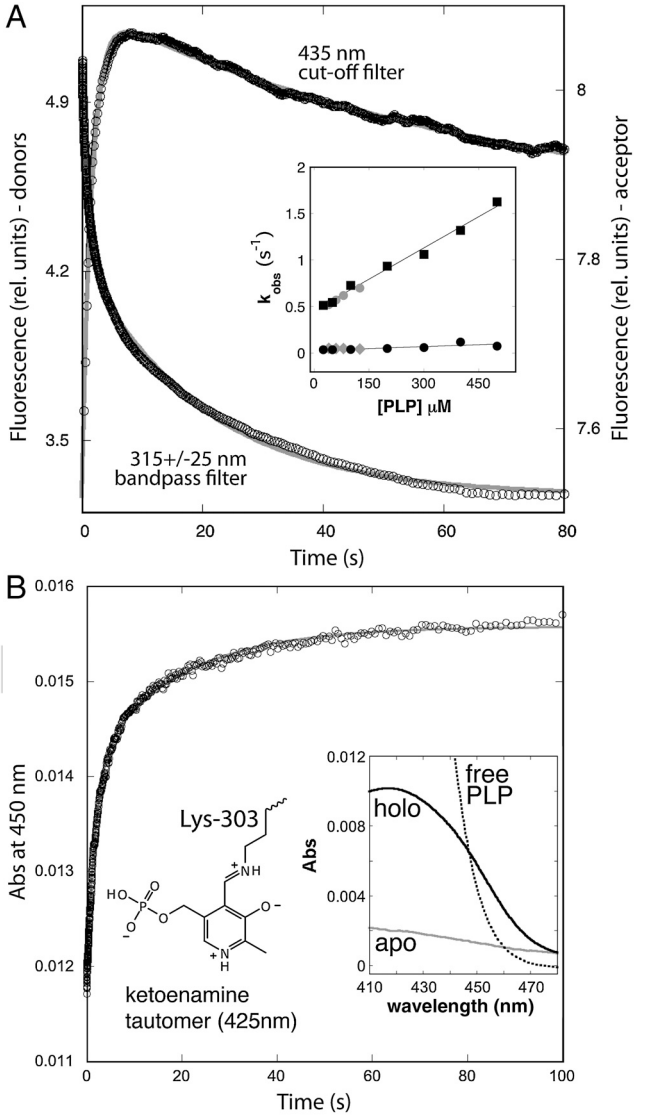

Fig. 3. Kinetics of PLP binding to apo-hDDC. (*A*): typical experimental traces recorded monitoring respectively: *lower trace*—the fluorescence of the donors (aromatic residues) recorded with a bandpass 315 + / – 25 nm filter; *upper trace*—the fluorescence of the acceptor (PLP) recorded with a 435 nm cut-off filter. *Inset*: plot of the observed rate constants for the two kinetic phases as a function of PLP concentration, calculated respectively from the fluorescence (*black markers*) and the absorbance (*B*) (*gray markers*) experiment. Each point refers to an average of at least three repetitions and the typical experimental error on the k_{obs} was in the order of 5%. It is of particular interest to compare the data recorded by measuring the donors and acceptor fluorescence. In fact, while the fluorescence of the aromatic residues decreases in both the fast and slow phases, consistent with an energy transfer to the acceptor, the fluorescence of the PLP decreases only in the slow phase. The latter behavior is clearly inconsistent with a simple FRET and could only be explained by postulating a conformational change of the protein. (*B*): trace obtained by recording the absorbance of the internal aldimine (ketoenamine tautomer) at 450 nm. *Inset*: reference spectra of 4 μM apo and holo-hDDC; 40 μM free PLP.

escence emission. In all cases, the observed kinetics displayed a biphasic behavior (Fig. 3*A*). Overall, whereas the rate constant for the fast phase appears to increase linearly with increasing ligand concentration (Fig. 3*A* inset, black squares), the rate constant for the slow phase is essentially independent of PLP concentration (black circles). This result indicates the presence of a monomolecular reaction following initial ligand recognition, consistent with a conformational change occurring after the initial binding of PLP to the apoenzyme.

We next performed single wavelength stopped-flow experiments recording the absorbance of the sample at 450 nm (Fig. 3*B*). Under these conditions, we monitored the formation and local environment of the Schiff base between the PLP and the ϵ-nitrogen of Lys-303 of the apoenzyme. The PLP-Lys-303 Shiff base undergoes a keto-enol tautomeric equilibrium with the ketoenamine and the enolimine tautomers peaking at 425 and 335 nm, respectively. The ratio between the two species is affected by the chemical environment and by pH (21, 27). In the absorbance experiment at 450 nm, where we only monitor the formation of the ketoenamine tautomer (28, 29), we observed the same two phases as in the FRET experiments (the observed rate constants as a function of PLP concentration are plotted in the inset of Fig. 3*A*—gray markers). This result indicates that the fast and slow kinetic phases cannot be assigned to (*i*) a first encounter between PLP and the enzyme followed by (*ii*) the formation of the Schiff base.

Overall, our kinetic analysis suggests the existence of a complex mechanism whereby cofactor binding and Schiff base formation occur simultaneously in the fast phase, which depends on PLP concentration. These events are followed by a major conformational change, whose apparent kinetics does not depend on cofactor concentration, and where the local environment of PLP is altered, as detected by absorbance and emission properties of the complex.

Discussion

The structure of apo-hDDC indicates that this protein, which has been considered to date as a tightly associated dimer, is able to assume an open conformation. This evidence, while explaining data indicating that a large conformational transition is occurring to Group II decarboxylases upon PLP binding (18–21), forces to reconsider the mechanism of cofactor addition as well as the data available on the preferential degradation of the apoenzymes in a new perspective.

The crystals of the asymmetric dimer of the open DDC allowed us to take structural snapshots of the cofactor-free apoprotein and of three alternative conformation of the active site at different PLP saturations (Fig. 2). In the fourth conformation (Fig. 2*D*: chain-A—structure 2) PLP is covalently bound through the Shiff base and loop1 is in the holo conformation. This evidence indicates that complete achievement of the closed conformation of the dimer is not essential for Shiff base formation and that PLP binding to the intermediate monomer is able to induce rearrangement of loop1. On the other hand, it is also evident that covalent binding of the cofactor can only be achieved after an initial rearrangement towards the closed conformation, because, even at saturating PLP concentration, no Shiff base is observed in the active site of the open monomer (Fig. 2*B*: chain-B—structure 2).

Coupling the structural analysis with the kinetic experiments, our data strongly suggest that PLP binding to the open structure, which may exist in solution as a dynamic ensemble of conformations, triggers an initial conformational change at the level of the active site yielding the rearrangement of loop1 that favors the transition to the closed conformation. Because loop1 in the closed conformation is making direct interaction with loop2 of the partner subunit (residues 100′ to 110′) which in turn contacts the flexible loop (also of the other subunit—loop3′), as illustrated in Fig. 4, Movie S3, we think that the conformational change of loop1 is transmitted to loop2′ and then to loop3′.

Indeed both loop2 and 3 in the open conformation of hDDC are solvent exposed and appear to be mobile and therefore not visible in the electron density of both subunits, while in the closed form of the enzyme they are buried and well structured (with the exception of 13 residues of the flexible loop). The hypothesis that loop1 acts as a conformational relay and can be considered as a key structural element is also confirmed by the architecture of the small C-domain. The backbone of loop1, in fact, makes a double turn due to the presence of Pro-74. This conformation is further stabilized by an additional aromatic stacking interactions with residues belonging to the C-domain (Fig. 4). The double turn allows Trp-71, and other residues of loop1, to interact directly with loop2′ by forming an hydrophobic cluster comprising, among other residues, Phe-103′ and Tyr-79 as shown in Fig. 4. Notice that loop1, loop2 (in particular Phe-103), and the flexible loop all contain residues involved in substrate binding (25, 30, 31); indicating that the structural rearrangement described here and the enzyme catalytic activity are tightly interconnected. Furthermore, of the 23 point mutations of DDC identified in patients with various neurotransmitters disorders 16 are part of the structural determinants involved in the conformational change that we propose, or make direct interaction with them (Table S1). In

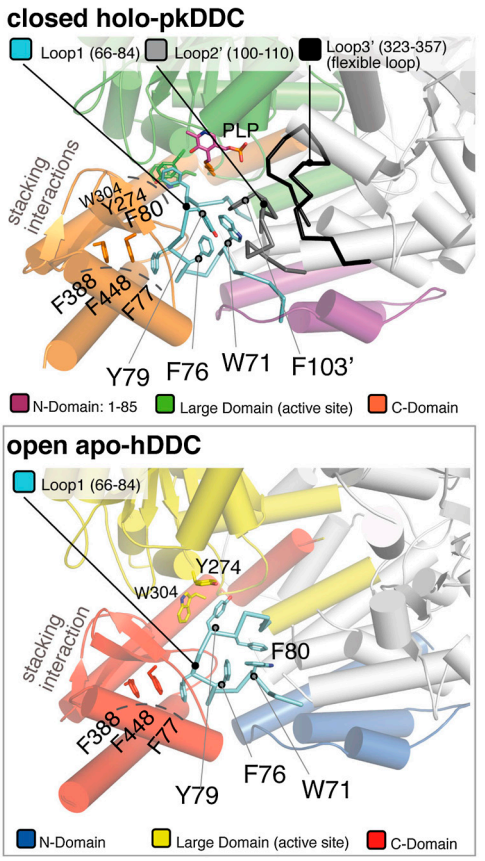

Fig. 4. Proximity relation of loop1 with loop2 and the flexible loop. The top box is a cartoon representation of the closed-holo-pkDDC dimer (Pdb id: 1js6) illustrating the proximity relation of loop1 (*Cyan*) with loop2 (*Gray*) and the flexible loop (*Black*) of the partner monomer. The three domains are colored as in Fig. 1. In this structure, loop1 (*Cyan*) directly interacts with loop2′ (*Gray*) which in turn contacts the flexible loop3′ (*Black*). The position of some important residues of loop1 in the holo state (i.e. Tyr-79 and Trp-71) and the position of the two aromatic stacking interactions (Phe-80 with Tyr-274 and Trp-304 of the large domain and of Phe-77 with Phe-388 and Phe-448 from the C-domain) is also shown. Notice that in the structure of the open-apo-form of hDDC (bottom box), due to the separation of the two subunits, the residues of loop2 and of the flexible loop are not visible, and only the aromatic stacking interaction with the residues of the C-domain is conserved.

particular, eight of these mutants belong to or contact loop1. Among them, the Y79C mutant appears particularly significant becauseTyr-79, which switches position with Phe-80 when loop1 changes conformation from the apo to the holoenzyme, is one of the key residues in our proposed mechanism.

This study allows us to speculate over a debated aspect of the mechanism of PLP addition to the apoenzyme. It has been proposed that, in the cell, PLP is directly transferred from pyridoxal kinase (PLK) to the apoenzyme by a channeling mechanism (32) but, although direct interaction between PLK and apoGAD has been demonstrated (33), the only access to the active site in the closed pkDDC dimer is a small 7 Å wide positively charged gorge (Fig. S5). The open conformation described here is therefore the form of the enzyme most likely able to interact with PLK, because the active site in this conformation is solvent exposed and easily accessible (Fig. 1). In this sense it is tempting to speculate on the astonishing structural complementarity between the PLK dimer and the huge cleft of the open-apo-hDDC structure: in a putative complex between the two proteins the two PLP molecules bound to PLK would face exactly the active sites of the open DDC (Fig. S6).

Finally, our results shed light on another crucial issue: there is evidence that apoDDC and apoGAD are selectively degraded in vivo. ApoDDC is degraded at least 20-fold faster than the holoenzyme in rat brain cells (11), while it has been demonstrated that holoGAD has a much higher stability than apoGAD (20). Indeed preferential degradation by the ubiquitin-proteosome system (UPS) has been suggested for apoDDC and demonstrated for apo tyrosine aminotransferase (13, 32). On the basis of the holo structures available for these enzymes (25, 30) these data could hardly be interpreted and most of the current hypothesis focuses on the mobility of the flexible loop. On the contrary, the existence of the open structure of hDDC would allow to present a structural interpretation of the lower stability of the apoenzymes in vivo. Indeed it is accepted that ubiquitylation is often driven by conformational and/or by an order-disorder transition. In particular, ubiquitin-ligases recognize unstructured zones of the target protein, or newly exposed surfaces. The opening of the apo-hDDC dimer implies that: (*i*) the solvent accessible surface area increases of 14%, (*ii*) the active site and a large part of the dimer interface becomes exposed, (*iii*) three important loops become mobile or unstructured and, (*iv*) the global enzyme volume and shape changes. Based on these observations, we propose a simple mechanism where the UPS regulates the levels of the total enzyme in the CNS, based on PLP availability (Fig. 5). In this hypothesis, which will need further experimental evidence, the concentration of PLP in the brain is directly affecting the ratio between holo and apoenzyme which, because of their different conformation, may have different fates within the cell.

Materials and Methods

DDC Expression and Purification. Human DDC was heterologously expressed in *Escherichia coli* and purified as described in ref. 34. The apoenzyme was prepared as described in ref. 34.

Crystallization and Data Collection. Single crystals of hDDC were grown at 21 °C by hanging drop vapor diffusion method; 1 μL of protein solution (holo-hDDC 5 mg/mL in 50 mM Hepes pH 7.4 buffer) was mixed with 1 μL of reservoir (500 μL containing 0.1 M Hepes pH 7.0 and 28–30% Jeffamine ED 2001 pH 7.0). Crystal grew in 5–8 d. No cryoprotectant was used before flash freezing in liquid nitrogen. Data were collected to 2.9 Å resolution. Crystals belong to the tetragonal space group $P4_12_12$. Data were integrated/scaled using MOSFLM (35) and SCALA (36). The asymmetric unit (AU) contains two monomers (one noncrystallographic dimer) with a solvent content of 54%.

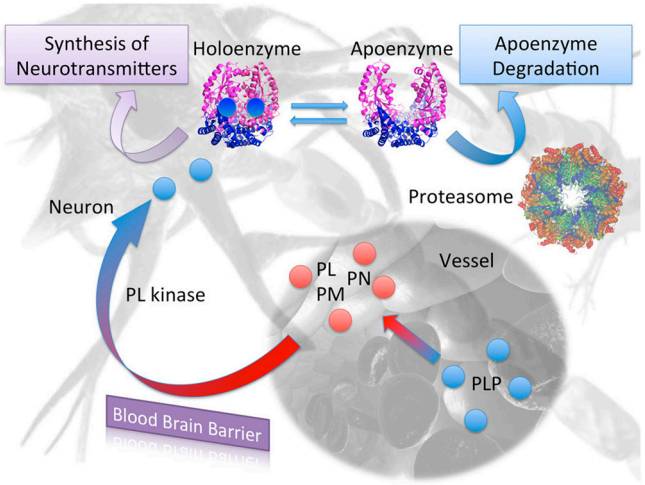

Fig. 5. Proposed regulatory model of DDC levels in the brain: Only Pyridoxal (PL), Pyridoxine (PN), or Pyridoxamine (PM) can cross the blood brain barrier, mostly at the choroid plexi. PLP is first cleaved to pyridoxal by nonspecific membrane-associated alkaline phosphatases. Once in the brain cell, B_6 vitamers are converted again in PLP by PL kinase, and directly or indirectly transferred to apoenzymes. PLP transfer may be facilitated by the open conformation of the apoenzyme presented in the present paper. The active holoform is responsible for the synthesis of biogenic amines, while the apo- open conformation, which exposes a wider protein surface and has more unstructured regions (loop2 and the flexible loop), is recognized by ubiquitin ligases and preferentially degraded by the ubiquitin proteasome system (UPS).

Crystals of the open hDDC with 1.5 equivalents of PLP bound (structure-2, Fig. 2) and no PLP bound (structure-3, Fig. 2) were obtained by soaking the previous described crystals in a solution containing 0.1 M Hepes pH 7.0; 15% Jeffamine ED 2001 pH 7.0; 5 mM PLP for 72 h and in a 2 μL droplet of reservoir for 24 h respectively. Diffraction data were collected up to 2.8 Å and 3.2 Å for the +PLP and −PLP crystals respectively. See Table S2 for complete data collection statistics.

Phasing and Refinement. Phases were obtained by Molecular Replacement method with MOLREP (37) using one monomer of the holo-pkDDC as search model (PDB id: 1js6).

Building and refinement was iteratively carried out using COOT (38) and REFMAC5 (39). ~~Nonvisible~~ side chain atoms were included in the final model with zero occupancy only for residues with visible main chain atoms, otherwise the entire residue was omitted. The geometrical quality of the three models was assessed using PROCHECK (40) and MolProbity (41). Final statistics are reported in Table S2.

PLP Binding to apo-hDDC. The time evolution of binding to PLP was followed on a stopped-flow apparatus by monitoring either the absorbance at 450 nm or the fluorescence emission (exciting the sample at 280 nm and monitoring emission using either a 315 ± 25 nm band pass or a 435 nm cut-off filter). Enzyme concentration (monomer) after mixing was 4 μM and 1 μM respectively for the single wavelength and the fluorescence experiment. Measurements were performed on an SX18-MV stopped-flow instrument (Applied Photophysics) using symmetric mixing. The traces were recorded in 100 mM Hepes buffer at pH 7.4, at 25 °C.

Kinetic traces were extracted and analyzed using Kaleidagraph software package.

ACKNOWLEDGMENTS. We thank European Synchrotron Radiation Facility (ESRF) and Berliner Elektronenspeicherring-Gesellschaft für Synchrotronstrahlung (BESSY) staff for beam time allocation and for technical assistance. Maurizio Brunori, Anna Tramontano and Roberto Contestabile (Rome, IT) are also gratefully acknowledged for critical reading of the manuscript. Funds from the Ministero della Università of Italy [RBRN07BMCT, 20094BJ9R7_001] and from the University of Rome La Sapienza to F.C. are gratefully acknowledged. This study was also supported by funds from MIUR (Prin 2007) to C.B.V.

1. Lanoue AC, Dumitriu A, Myers RH, Soghomonian JJ (2010) Decreased glutamic acid decarboxylase mRNA expression in prefrontal cortex in Parkinson's disease. *Exp Neurol* 226:207–217.

2. Kontos CK, Papadopoulos IN, Fragoulis EG, Scorilas A (2010) Quantitative expression analysis and prognostic significance of L-DOPA decarboxylase in colorectal adenocarcinoma. *Br J Cancer* 102:1384–1390.

3. Karolewicz B, et al. (2010) Reduced level of glutamic acid decarboxylase-67 kDa in the prefrontal cortex in major depression. *Int J Neuropsychoph* 13:411–420.
4. Ercan-Sencicek AG, et al. (2010) L-histidine decarboxylase and Tourette's syndrome. *N Engl J Med* 362:1901–1908.
5. Abdel-Salam OM (2008) Drugs used to treat Parkinson's disease, present status and future directions. *CNS Neurol Disord-Dr* 7:321–342.
6. Blechingberg J, Holm IE, Johansen MG, Borglum AD, Nielsen AL (2010) Aromatic l-amino acid decarboxylase expression profiling and isoform detection in the developing porcine brain. *Brain Res* 1308:1–13.
7. Kitahama K, et al. (2009) Aromatic L-amino acid decarboxylase-immunoreactive structures in human midbrain, pons, and medulla. *J Chem Neuroanat* 38:130–140.
8. Guilarte TR, Wagner HNJ, Frost JJ (1987) Effects of perinatal vitamin B6 deficiency on dopaminergic neurochemistry. *J Neurochem* 48:432–439.
9. Siow YL, Dakshinamurti K (1985) Effect of pyridoxine deficiency on aromatic L-amino acid decarboxylase in adult rat brain. *Exp Brain Res* 59:575–581.
10. Rahman MK, et al. (1982) Effect of pyridoxal phosphate deficiency on aromatic L-amino acid decarboxylase activity with L-DOPA and L-5-hydroxytryptophan as substrates in rats. *Jpn J Pharmacol* 32:803–811.
11. Matsuda N, Hayashi H, Miyatake S, Kuroiwa T, Kagamiyama H (2004) Instability of the apo form of aromatic L-amino acid decarboxylase in vivo and in vitro: implications for the involvement of the flexible loop that covers the active site. *J Biochem* 135:33–42.
12. Allen GF, et al. (2010) Pyridoxal 5′-phosphate deficiency causes a loss of aromatic L-amino acid decarboxylase in patients and human neuroblastoma cells, implications for aromatic L-amino acid decarboxylase and vitamin B(6) deficiency states. *J Neurochem* 114:87–96.
13. Allen GF, Land JM, Heales SJ (2009) A new perspective on the treatment of aromatic L-amino acid decarboxylase deficiency. *Mol Genet Metab* 97:6–14.
14. Myers MA, et al. (2003) A diabetes-related epitope of GAD65: a major diabetes-related conformational epitope on GAD65. *Ann N Y Acad Sci* 1005:250–252.
15. di Salvo ML, Contestabile R, Safo MK (2011) Vitamin B(6) salvage enzymes: Mechanism, structure and regulation. *Biochim Biophys Acta* 1814:1597–1608.
16. Li MH, et al. (2002) Crystal structure of brain pyridoxal kinase, a novel member of the ribokinase superfamily. *J Biol Chem* 277:46385–46390.
17. Clayton PT (2006) B6-responsive disorders: a model of vitamin dependency. *J Inherit Metab Dis* 29:317–326.
18. Moya-Garcia AA, Medina MA, Sanchez-Jimenez F (2005) Mammalian histidine decarboxylase: from structure to function. *Bioessays* 27:57–63.
19. Rodriguez-Caso C, et al. (2003) Local changes in the catalytic site of mammalian histidine decarboxylase can affect its global conformation and stability. *Eur J Biochem* 270:4376–4387.
20. Chen CH, Wu SJ, Martin DL (1998) Structural characteristics of brain glutamate decarboxylase in relation to its interaction and activation. *Arch Biochem Biophys* 349:175–182.
21. Moore PS, Dominici P, Borri Voltattorni C (1996) Cloning and expression of pig kidney dopa decarboxylase: comparison of the naturally occurring and recombinant enzymes. *Biochem J* 315:249–256.
22. Schneider G, Kack H, Lindqvist Y (2000) The manifold of vitamin B6 dependent enzymes. *Structure* 8:R1–6.
23. Sandmeier E, Hale TI, Christen P (1994) Multiple evolutionary origin of pyridoxal-5′-phosphate-dependent amino acid decarboxylases. *Eur J Biochem* 221:997–1002.
24. Fenalti G, et al. (2007) Molecular characterization of a disease associated conformational epitope on GAD65 recognized by a human monoclonal antibody b96.11. *Mol Immunol* 44:1178–1189.
25. Burkhard P, Dominici P, Borri-Voltattorni C, Jansonius JN, Malashkevich VN (2001) Structural insight into Parkinson's disease treatment from drug-inhibited DOPA decarboxylase. *Nat Struct Biol* 8:963–967.
26. Dominici P, Moore PS, Castellani S, Bertoldi M, Voltattorni CB (1997) Mutation of cysteine 111 in Dopa decarboxylase leads to active site perturbation. *Protein Sci* 6:2007–2015.
27. Zhou X, Toney MD (1999) pH studies on the mechanism of the pyridoxal phosphate-dependent dialkylglycine decarboxylase. *Biochemistry* 38:311–320.
28. Hill MP, Carroll EC, Toney MD, Larsen DS (2008) Rapid photodynamics of vitamin B6 coenzyme pyridoxal 5′-phosphate and its Schiff bases in solution. *J Phys Chem B* 112:5867–5873.
29. Malerba F, Bellelli A, Giorgi A, Bossa F, Contestabile R (2007) The mechanism of addition of pyridoxal 5′-phosphate to *Escherichia coli* apo-serine hydroxymethyltransferase. *Biochem J* 404:477–485.
30. Fenalti G, et al. (2007) GABA production by glutamic acid decarboxylase is regulated by a dynamic catalytic loop. *Nat Struct Mol Biol* 14:280–286.
31. Bertoldi M, Gonsalvi M, Contestabile R, Voltattorni CB (2002) Mutation of tyrosine 332 to phenylalanine converts dopa decarboxylase into a decarboxylation-dependent oxidative deaminase. *J Biol Chem* 277:36357–36362.
32. Kim YT, Kwok F, Churchich JE (1988) Interactions of pyridoxal kinase and aspartate aminotransferase emission anisotropy and compartmentation studies. *J Biol Chem* 263:13712–13717.
33. Cheung PY, et al. (2003) Interaction between pyridoxal kinase and pyridoxal-5-phosphate-dependent enzymes. *J Biochem* 134:731–738.
34. Montioli R, Cellini B, Borri Voltattorni C (2011) Molecular insights into the pathogenicity of variants associated with the aromatic amino acid decarboxylase deficiency. *J Inherit Metab Dis*, Epub ahead of print. (doi: 10.1007/s10545-011-9340-6).
35. Leslie AGW (1992) Mosflm. *Joint CCP4 and ESF-EACBM newsletter on protein Crystallography* 26:27–33.
36. Evans PR (1997) Scala. *Joint CCP4 and ESF-EACBM newsletter on protein Crystallography* 33:22–24.
37. Vagin A, Teplyakov A (2010) Molecular replacement with MOLREP. *Acta Crystallogr D* 66:22–25.
38. Emsley P, Cowtan K (2004) COOT: model-building tools for molecular graphics. *Acta Crystallogr D* 60:2126–2132.
39. Murshudov GN, Vagin AA, Dodson EJ (1997) Refinement of macromolecular structures by the maximum-likelihood method. *Acta Crystallogr D* 53:240–255.
40. Laskowski RA, MacArthur MW, Moss DS, Thornton JM (1993) PROCHECK: a program to check the stereochemical quality of protein structures. *J Appl Crystallogr* 26:283–291.
41. Davis IW, et al. (2007) MolProbity: all-atom contacts and structure validation for proteins and nucleic acids. *Nucleic Acids Res* 35:W375–83.

Supporting Information

Giardina et al. 10.1073/pnas.1111456108

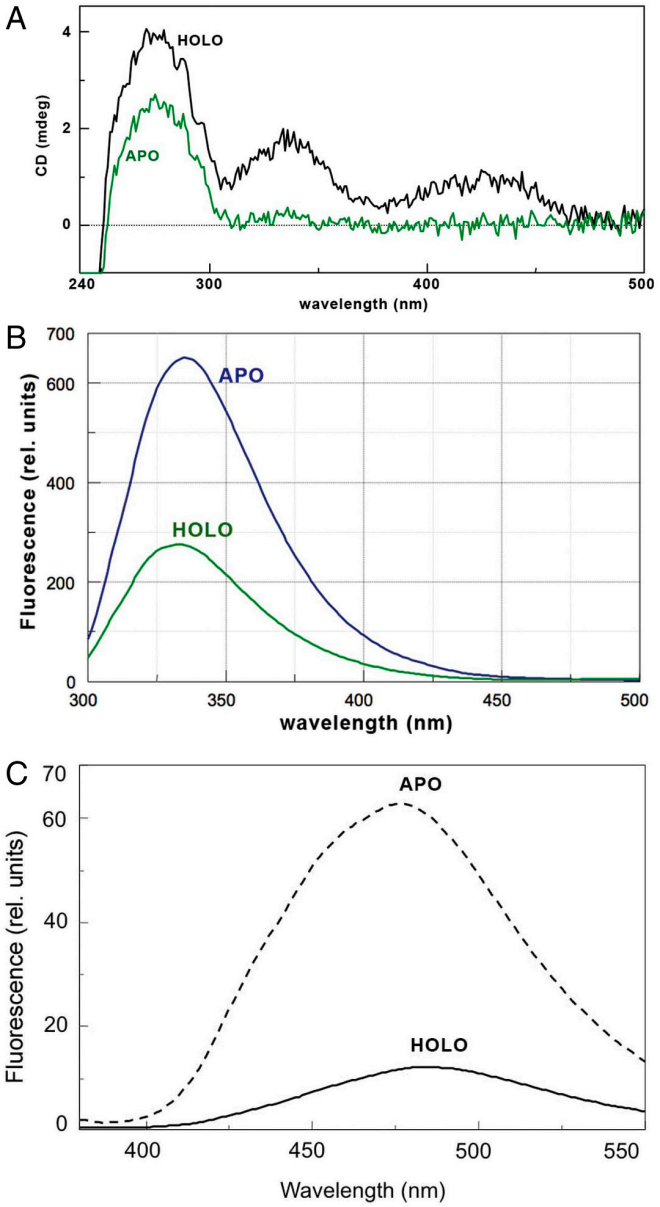

Fig. S1. Near-UV CD spectra, intrinsic and ANS fluorescence spectra of holo and apo-hDDC. (*A*). Near-UV and Vis CD spectra of 5 μM holo (*Black*) and apoenzyme (*Green*). (*B*). Fluorescence emission spectra of 1 μM holo (*Green*) and apoenzyme (*Blue*). Excitation at 280 nm (*C*). Fluorescence emission spectra of 1 μM holo (–) and apoenzyme (- - -) incubated in the presence of 15 μM 8-Anilino-1-naphthalenesulfonate (ANS) at 25 °C for 1 h, registered upon excitation at 365 nm. All measurement were made in 0.1M Potassium Phosphate buffer pH = 7.4.

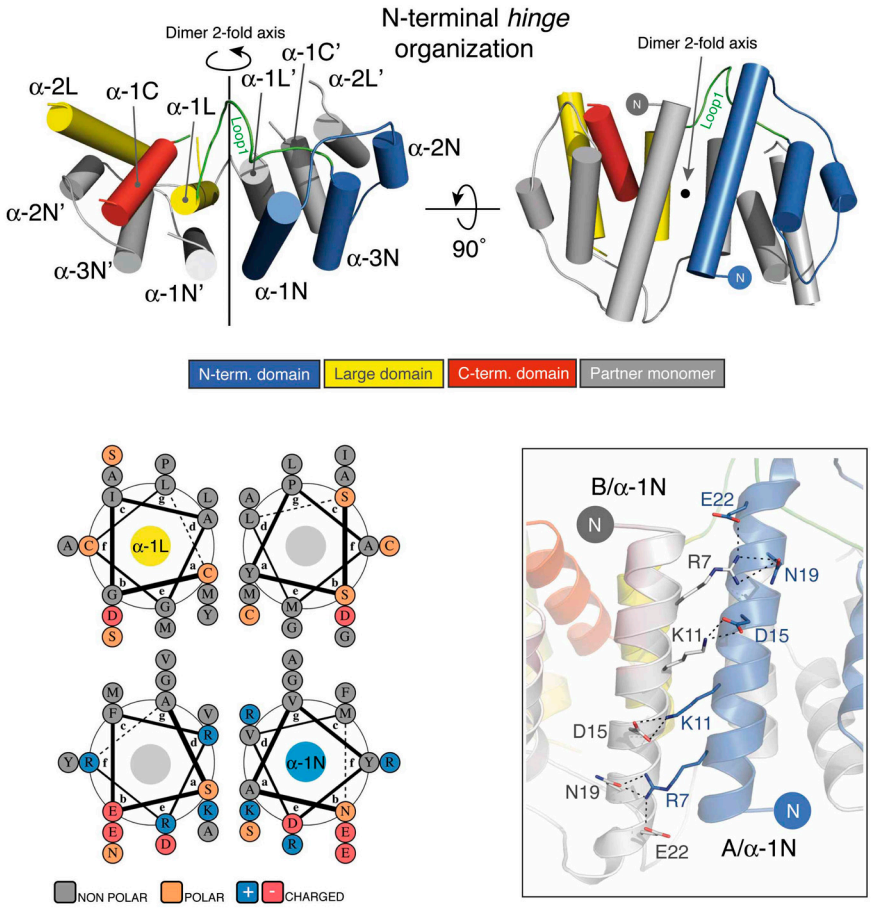

Fig. S2. Structural organization of the N-terminal hinge (the dimer interface). Organization of the 12 helices cluster that arises from the domain swapping of the N-terminal domain which is peculiar of the Group II decarboxylases. These helices are organized as an extended four helix bundle network and build the dimer interface; i.e., the hinge of the bivalve shell (see Fig. 1). Color code: *Blue*—N-terminal domain; *Yellow*—Large domain; *Red*—Small domain; residues that are not part of the interface were removed for clarity. The capital letters used after the helix number denote the domain to which each helix belongs (i.e., α-1N—N-terminal, α-1L—Large, α-1C—C-terminal). The lower part of the figure shows a helical-wheel diagram and a cartoon representation of the central four helix bundle (α-1N − α-1L + α-1N′ − α-1L′) illustrating the strong hydrophobic interaction of the core and the network of hydrogen bonds of the surface residues.

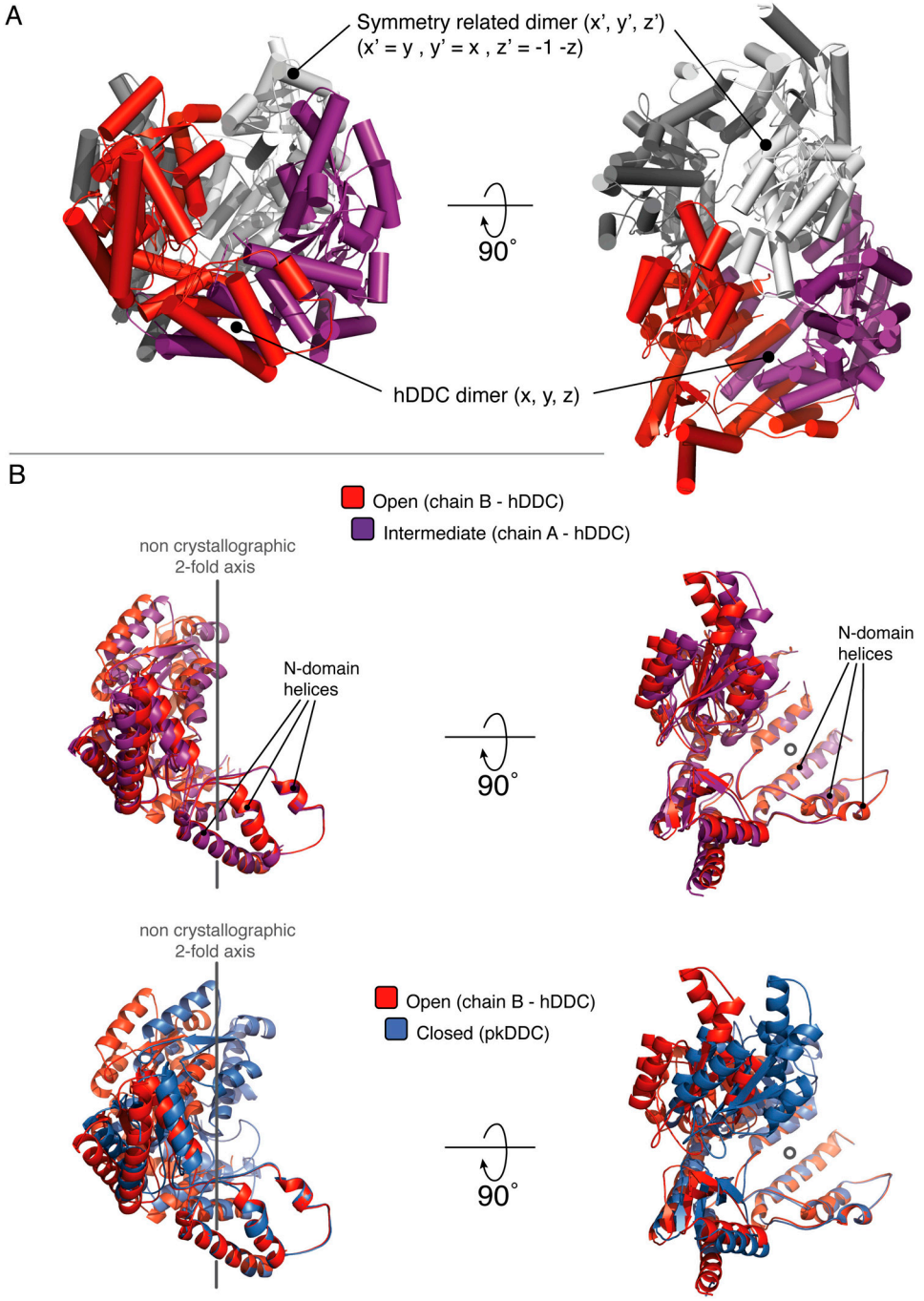

Fig. S3. Intermolecular crystal contacts and asymmetry of the two dimer subunits. (*A*). Tetrameric assembly of hDDC in the crystal lattice. Each dimer in the open conformation *bites* a symmetry related mate, corresponding to the equivalent position *y*, *x*, *-z* of an adjacent cell. The space group is $P4_12_12$. (*B*). Top—Superposition of the two monomers of hDDC on the N-domain helices (*Red*: chain-B; *Purple*: chain-A) reveals that the structure of the two subunits is not symmetrical, with chain-A being more closed than chain-B. The monomers are shown in the same orientation as in (*A*). *Bottom*—superposition, on the N-domain helices, of the open monomer (chain-B) of hDDC (*Red*) with the pkDDC (pdb id: 1JS6) closed monomer (*Blue*). Open, Intermediate and Closed refer to the different conformations of the monomer as illustrated in Fig. 2.

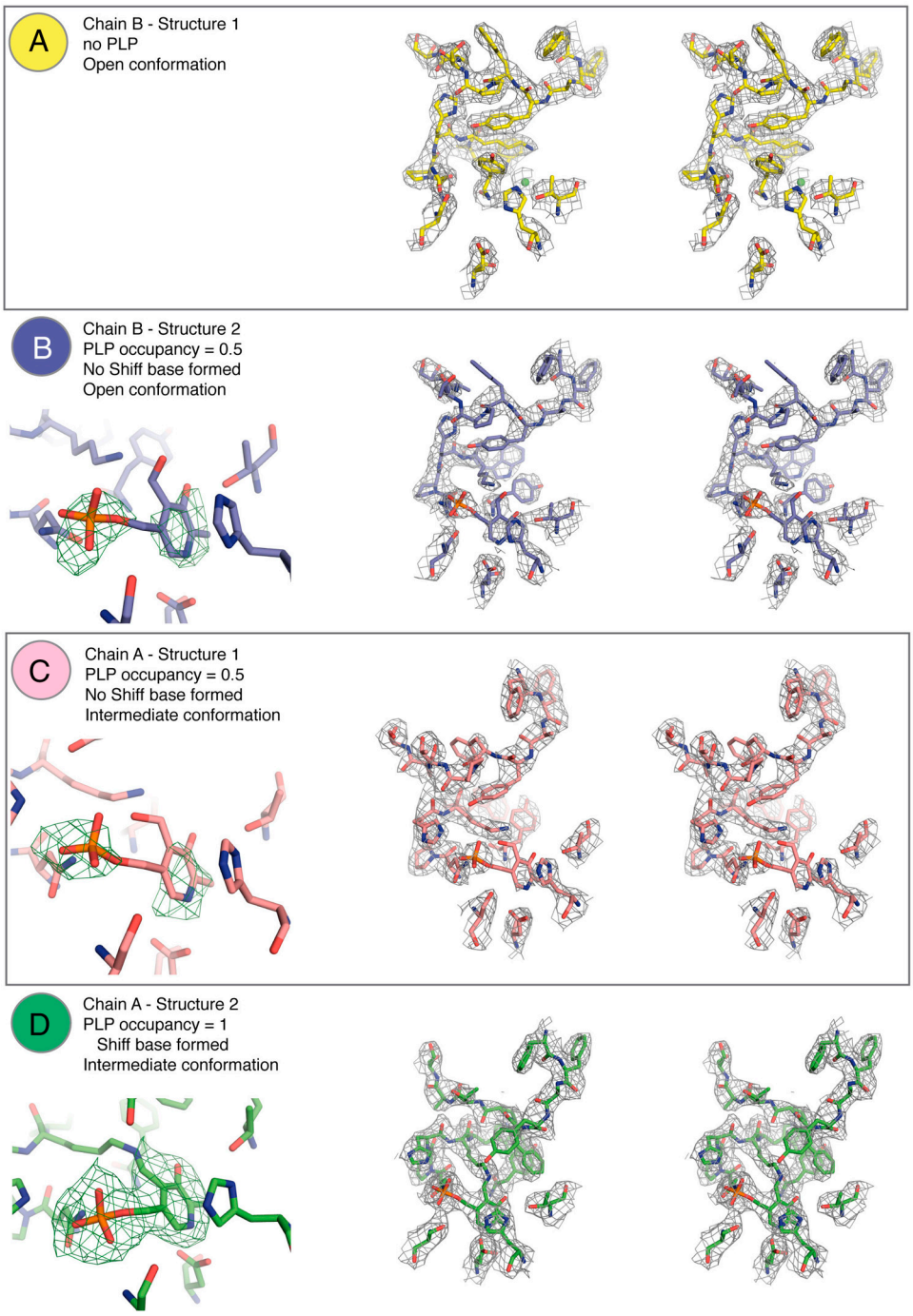

Fig. S4. Electron density of the alternative conformations of the active site. On the *left*: Fo-Fc omit map calculated for PLP and contoured at 2.0σ. On the *right*: Stereo representation of the 2Fo-Fc map contoured at 1.3σ.

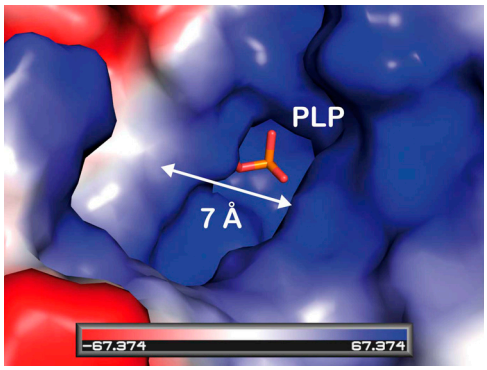

Fig. S5. Access to the active site in the closed pkDDC dimer. Surface representation colored by electrostatic potential of the active site access in the closed conformation (pkDDC—pdb id: 1js6). Only the phosphate group of the cofactor is visible inside the 7 Å wide gorge.

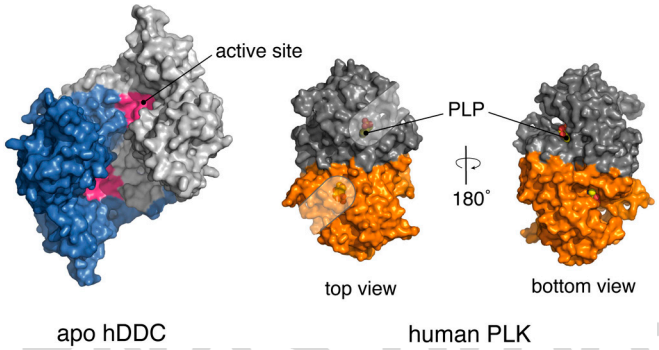

Fig. S6. Structural complementarity between the PL Kinase (PLK) dimer and the open apo-hDDC. On the *left*, a top view of the open apo-hDDC dimer showing the position of the exposed active sites (*magenta*); on the *right*, top and bottom views of the human PLK dimer (pdb id: 3keu). The transparency in the top view illustrates the position of the PLP and the direction of the access channels to the substrate binding site, which are visible in the bottom view. In a possible complex between the two proteins the two PLP molecules bound to PLK would face exactly the active sites of DDC.

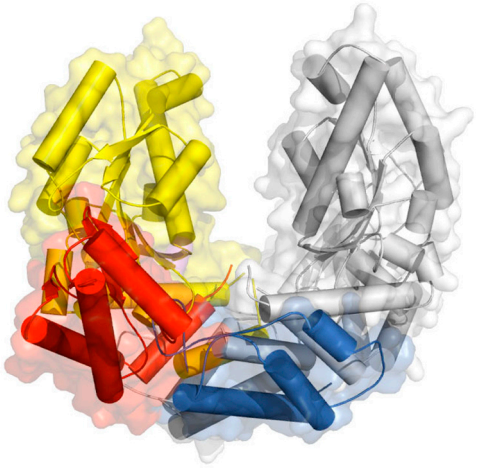

Movie S1. Domain organization of the apo hDDC dimer. The first part of the animation shows the Tertiary and Quaternary structure of the apo-hDDC dimer in the open conformation. The second part illustrates the organization of the dimer's hinge; the domain swapping of the N-domains.

Movie S1 (MOV)

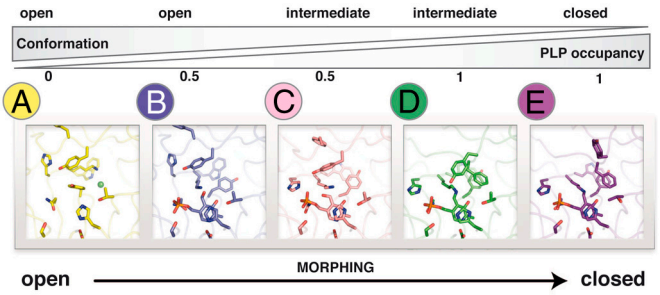

Movie S2. Five step morphing through the alternative conformations of the active site of DDC. The animations is a five step morphing through the different conformations of the active site of DDC as ordered in Fig. 2. Letters corresponding to the five different states appear (top left corner) each time the morphing corresponds to a crystal structure. Notice that morphing is a simple animation from the starting coordinates to the ending coordinates. No kinetic, thermodynamic or molecular dynamic calculation is employed.

Movie S2 (MOV)

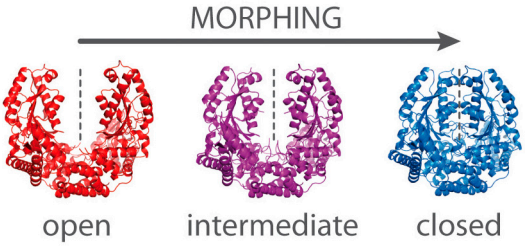

Movie S3. Morphing through the different monomer conformations of DDC. The animation shows the morphing from an hypothetical symmetric dimer with both monomers in the open conformation (*Red*) to the closed conformation (*Blue*—pkDDC structure), passing through the intermediate conformation (*Purple*). The second part of the movie focuses on the conformational transition of loop1, after PLP binding, followed by folding of the mobile loop2 and loop3 residues, which are structured only in the closed conformation. Notice that during the animation, for technical reasons, PLP is not morphing together with the protein and its position, in the starting and ending points, is shown only for clarity. Notice that morphing is a simple animation from the starting coordinates to the ending coordinates. No kinetic, thermodynamic or molecular dynamic calculation is employed.

Movie S3 (MOV)

Table S1. List of 23 point mutation of DDC identified in patients with various neurotransmitters disorders. The mutations are taken from BIOMDB database (http://www.biopku.org/BioPKU_databasesBIOMDB.asp). Mutants which are part or make direct interaction with the structural determinants involved in the conformational change discussed in the paper are highlighted. A brief description of their role or nature of the interaction is also provided

Mutation	Position	Interaction	Type of interaction (conformation)
Y79C	Loop1		swapping position with F80 going from the apo to the holo state
H72Y	Loop1		adjacent to W71 (see Fig. 4)
T69M	Loop1		same as above
H70T	Loop1		same as above
R462P		Loop1	H-bond with Y75 (open)
R447H		Loop1	H-bond with the C = O of Y79 (closed)
E25K		Loop1	interacting with Y75 (closed)
L408I		Loop1	interacting with F80 (closed)
G102S	Loop2		involved in substrate binding
A110Q	Loop2		
F309L		Loop2 Loop3	involved in substrate binding; contacts both Loop2 and Loop3 residues in the closed structure; it is mobile in the open structure
R347Q	Loop3		involved in substrate binding
R358H	Loop3		H-bond with D310 of the catalytic Loop (open)
R7X	N-ter. Hinge (α-1N)		H-bond with N19 and E22 (see Fig. 2)
A91V	N-ter. Hinge (α-1L)		hydrophobic core of the central 4-helix bundle
L38P	N-ter. Hinge (α-2N)		disruption of α-2N
P47H			
S147R			
S250F			
A275T			
R285W			
V460G			
R412W			

Table S2. Data collection and refinement statistics for structure 1–3 (see Fig. 2)

	Structure 1	Structure 2	Structure 3
Coordinates	3RBF	3RCH	3RBL
Data collection *			
Beamline	BESSY (BL-1)	ESRF (ID14-1)	ESRF (ID14-1)
Space group	$P4_12_12$	$P4_12_12$	$P4_12_12$
Cell dimensions			
$a = b,c$ (Å)	175.84, 74.96	177.00, 74.83	179.64, 74.95
Resolution (Å)	2.90 (3.06–2.90)	2.80 (2.95–2.80)	3.25 (3.40–3.25)
R_{sym} or R_{merge}	11.2 (47.9)	13.3 (61.2)	13.1 (40.1)
$I/\sigma I$	15.7 (3.6)	13.6 (3.5)	13.8 (3.8)
Completeness (%)	99.3 (99.3)	100 (100)	99.8 (100)
Redundancy	8.8 (6.0)	7.1 (7.2)	6.4 (6.2)
Refinement			
Resolution (Å)	45.0–2.9	30.0–2.8	30.0–3.25
No. reflections	26,369	28,290	18,961
R_{work}/R_{free}	21.2/26.6	20.1/25.9	22.1/28.3
No. atoms			
Protein (chain A/B)	3,474/3,480	3,504/3,461	3,469/3,480
PLP (chain A/B)	16/–	15/16	
Ion	2		1
Water		28	
Mean B-factor (Å^2)			
Protein (chain A/B)	18.1/18.2	25.9/26.2	48.0/45.3
PLP (chain A/B)	35.2/–	34.8/34.9	
Ion	40.1		56.4
Water		16.8	
rmsd			
Bond lengths (Å)	0.011	0.011	0.011
Bond angles (°)	1.263	1.318	1.301
Ramachandran: n. residues (%)			
favored	710 (90.7)	699 (89.7)	721 (92.2)
allowed	71 (9.1)	78 (10.0)	60 (7.7)
disallowed	2 (0.3)	2 (0.3)	1 (0.1)
Molprobity scores (percentile)	2.62 (89th)	2.94 (69th)	2.83 (91st)

*Values in parentheses are for highest-resolution shell.

AUTHOR QUERIES

AUTHOR PLEASE ANSWER ALL QUERIES 1

Q: 1_Please review the information in the author contribution footnote carefully. Please make sure that the information is correct and that the correct author initials are listed. Note that the order of author initials matches the order of the author line per journal style. You may add contributions to the list in the footnote; however, funding should not be an author's only contribution to the work.

Q: 2_PNAS does not allow statements of novelty or priority. Please approve the edit from “new” to “unique.”

Q: 3_The prefix “non” is only hyphenated when before a proper noun, an animal, or a protein or antibody and when part of a multiple-word term.